

Cosmic-ray ionization of molecular clouds

Marco Padovani^{1,2}, Daniele Galli² and Alfred E. Glassgold³

¹ Dipartimento di Astronomia e Scienza dello Spazio, Università di Firenze, Largo E. Fermi 2, I-50125 Firenze, Italy
e-mail: padovani@arcetri.astro.it

² INAF-Osservatorio Astrofisico di Arcetri, Largo E. Fermi 5, I-50125 Firenze, Italy
e-mail: galli@arcetri.astro.it

³ University of California at Berkeley, Berkeley, CA, 94720 USA
e-mail: glassgol@berkeley.astro.edu

Preprint online version: October 24, 2018

ABSTRACT

Context. Low-energy cosmic rays are a fundamental source of ionization for molecular clouds, influencing their chemical, thermal and dynamical evolution.

Aims. The purpose of this work is to explore the possibility that a low-energy component of cosmic-rays, not directly measurable from the Earth, can account for the discrepancy between the ionization rate measured in diffuse and dense interstellar clouds.

Methods. We collect the most recent experimental and theoretical data on the cross sections for the production of H_2^+ and He^+ by electron and proton impact, and we discuss the available constraints on the cosmic-ray fluxes in the local interstellar medium. Starting from different extrapolations at low energies of the demodulated cosmic-ray proton and electron spectra, we compute the propagated spectra in molecular clouds in the continuous slowing-down approximation taking into account all the relevant energy loss processes.

Results. The theoretical value of the cosmic-ray ionization rate as a function of the column density of traversed matter is in agreement with the observational data only if either the flux of cosmic-ray electrons or of protons increases at low energies. The most successful models are characterized by a significant (or even dominant) contribution of the electron component to the ionization rate, in agreement with previous suggestions. However, the large spread of cosmic-ray ionization rates inferred from chemical models of molecular cloud cores remains to be explained.

Conclusions. Available data combined with simple propagation models support the existence of a low-energy component (below ~ 100 MeV) of cosmic-ray electrons or protons responsible for the ionization of molecular cloud cores and dense protostellar envelopes.

Key words. ISM: cosmic rays, clouds – atomic and molecular processes

1. Introduction

Cosmic-rays (CRs) play a key role in the chemistry and dynamics of the interstellar medium (ISM). First, CR particles are a primary source of ionization, competing with stellar UV photons (absorbed in a thin layer of ~ 4 magnitudes of visual extinction, McKee 1999) and X-rays produced by embedded young stellar objects (Krolik & Kallman 1983; Silk & Norman 1983). The ionization fraction in turn drives the chemistry of molecular clouds and controls the coupling of the gas with the Galactic magnetic field (for a good review of the chemistry that occurs in the ISM in response to CR ionization see Dalgarno 2006). Second, CRs represent an important source of heating for molecular clouds because the energy of primary and secondary electrons produced by the ionization process is in large part converted into heat by inelastic collisions with ISM atoms and molecules.

In general, the CR ionization rate in the interstellar gas depends on the relative amount of H, H_2 and He (Dalgarno, Yan & Liu 1999). The first theoretical determination of the CR ionization rate was performed for clouds made only by atomic hydrogen by Hayakawa, Nishimura & Takayanagi (1961). They assumed a proton specific intensity (hereafter, for simplicity, *spectrum*) proportional to the proton energy E_p for $0.1 \text{ MeV} < E_p < 10 \text{ MeV}$ and computed $\zeta^{\text{H}} \approx 4 \times 10^{-16} \text{ s}^{-1}$. Spitzer & Tomasko (1968) determined a value (actually a lower limit) of $\zeta^{\text{H}} \gtrsim 6.8 \times 10^{-18} \text{ s}^{-1}$ for HI clouds, assuming a CR proton

spectrum declining below $E_p \approx 50 \text{ MeV}$, and an upper limit of $\zeta^{\text{H}} \lesssim 1.2 \times 10^{-15} \text{ s}^{-1}$, taking into account an additional flux of $\sim 2 \text{ MeV}$ protons produced by supernova explosions. To obtain the CR ionization rate of molecular hydrogen, ζ^{H_2} , a useful approximation is $1.5\zeta^{\text{H}_2} \approx 2.3\zeta^{\text{H}}$ (Glassgold & Langer 1974), giving $\zeta^{\text{H}_2} \approx 10^{-17} \text{ s}^{-1}$, in agreement with the lower limit on ζ^{H} of Spitzer & Tomasko (1968). This value of ζ^{H_2} is often referenced as the “standard” CR ionization rate in molecular clouds.

A major problem in the determination of the CR ionization rate is that low-energy CRs are prevented from entering the heliosphere by the solar wind and the interplanetary magnetic field (solar modulation). In practice, Earth-based measurements of CR fluxes give no information on the interstellar spectrum of protons and heavy nuclei for energies below $\sim 1 \text{ GeV/nucleon}$. Solar modulation also suppresses the flux of low-energy CR electrons, that shows considerable fluctuations already at energies of 10–100 GeV (see e.g. Casadei & Bindi 2004). Since the cross section for ionization of molecular hydrogen by collisions with protons and electrons has a maximum at $\sim 10 \text{ keV}$ and $\sim 50 \text{ eV}$, respectively (see Sect. 2), it is clear that a knowledge of CR spectrum at low energies is an important limiting factor for an accurate calculation of the ionization rate in the ISM. A direct measurement of the shape of the CR spectrum at these energies will be possible only when spacecrafts such as *Pioneer* and *Voyager* are well beyond the heliopause, the outermost boundary for solar modulation effects, believed to lie at 100–150 AU from

the Sun (at present, both Voyagers have already crossed the solar wind termination shock at 85–95 AU from the Sun).

Over the last three decades, several values of ζ^{H} ranging from a few 10^{-17} s^{-1} to a few 10^{-16} s^{-1} have been obtained in diffuse interstellar clouds from measurements of the abundances of various chemical species, in particular OH (Black & Dalgarno 1977; Hartquist, Black, & Dalgarno 1978; Black, Hartquist, & Dalgarno 1978) and HD (van Dishoeck & Black 1986; Federman, Weber & Lambert 1996). However, the derived rates depend sensitively on several model assumptions, e.g. the value of specific chemical reaction rates and the intensity of the UV background. In dense molecular clouds, the determination of the CR ionization rate is made even more uncertain by the sensitivity of molecular abundances to the level of depletion of the various species and the role of small and large grains in the chemical network. The values of ζ^{H_2} derived by Caselli et al. (1998) in a sample of 23 molecular cloud cores (column density $N(\text{H}_2) \sim 10^{22} \text{ cm}^{-2}$) through DCO^+ and HCO^+ abundance ratios span a range of about two orders of magnitudes from $\sim 10^{-17} \text{ s}^{-1}$ to $\sim 10^{-15} \text{ s}^{-1}$, with a scatter that may in part reflect intrinsic variations of the CR flux from core to core. Finally, values of ζ^{H_2} of a few times 10^{-17} s^{-1} have been obtained in clouds of higher column density ($N(\text{H}_2) \sim 10^{23}\text{--}10^{24} \text{ cm}^{-2}$) like the envelopes surrounding massive protostellar sources (van der Tak & van Dishoeck 2000; Doty et al. 2002).

The discovery of significant abundances of H_3^+ in diffuse clouds (McCall et al. 1998), confirmed by follow-up detections (Geballe et al. 1999; McCall et al. 2003; Indriolo et al. 2007), has led to values of ζ^{H_2} larger by about one order of magnitude than both the “standard” rate and previous estimates based on the abundance of OH and HD in dense clouds. Given the relative simplicity of the chemistry of H_3^+ , it is now believed that diffuse clouds are characterized by CR ionization rates $\zeta^{\text{H}_2} \approx 2 \times 10^{-16} \text{ s}^{-1}$ or larger. This high value of ζ^{H_2} in the diffuse interstellar gas can be reconciled with the lower values measured in cloud cores and massive protostellar envelopes by invoking various mechanisms of CR screening in molecular clouds due to either self-generated Alfvén waves in the plasma (Skilling & Strong 1976; Hartquist, Doyle & Dalgarno; Padoan & Scalo 2005) or to magnetic mirror effects (Cesarsky & Völk 1978; Chandran 2000). An alternative explanation, based on the possible existence of a low-energy flux of CR particles, is that they can penetrate (and ionize) diffuse clouds but not dense clouds, as recently proposed by McCall et al. (2003; see also Takayanagi 1973 and Umebayashi & Nakano 1981). This latter scenario is explored quantitatively in the present paper.

In this paper, we concentrate on molecular clouds, where hydrogen is present mostly in molecular form and we can ignore ionization of atomic hydrogen. In Sect. 8 we then apply our results to diffuse clouds, where the fraction of hydrogen in molecular form $f = 2N(\text{H}_2)/[N(\text{H}) + 2N(\text{H}_2)]$ has a mean value $\langle f \rangle \approx 0.6$ (Indriolo et al. 2007), implying that the column densities of H and H_2 are almost equal. This is justified because the quantity directly measured (or estimated) in the diffuse clouds examined in Sect. 8 is the ionization rate of H_2 as derived from the measured abundance of H_3^+ .

The organization of the paper is the following. In Sect. 2, 3 and 4 we examine the ionization reactions of CR protons and electrons incident on H_2 and He and other channels of electron production; in Sect. 5 we discuss the assumed interstellar spectra of CR protons and electrons; in Sect. 6 we discuss the energy loss mechanisms for CRs; in Sect. 7 we compute the ionization rate as function of the column density in a cloud; in Sect. 8 we compare our results with the available estimates of the CR ion-

Table 1. CR reactions in molecular clouds

reaction	cross section	ref.
$p_{\text{CR}} + \text{H}_2 \rightarrow p_{\text{CR}} + \text{H}_2^+ + e$	$\sigma_p^{\text{ion.}}$	§2.1
$p_{\text{CR}} + \text{H}_2 \rightarrow \text{H} + \text{H}_2^+$	$\sigma_p^{\text{e. c.}}$	§2.3
$p_{\text{CR}} + \text{H}_2 \rightarrow p_{\text{CR}} + \text{H} + \text{H}^+ + e$	$\sigma_p^{\text{diss. ion.}}$	§3.1
$p_{\text{CR}} + \text{H}_2 \rightarrow p_{\text{CR}} + 2\text{H}^+ + 2e$	$\sigma_p^{\text{doub. ion.}}$	§3.2
$e_{\text{CR}} + \text{H}_2 \rightarrow e_{\text{CR}} + \text{H}_2^+ + e$	$\sigma_e^{\text{ion.}}$	§2.2
$e_{\text{CR}} + \text{H}_2 \rightarrow e_{\text{CR}} + \text{H} + \text{H}^+ + e$	$\sigma_e^{\text{diss. ion.}}$	§3.1
$e_{\text{CR}} + \text{H}_2 \rightarrow e_{\text{CR}} + 2\text{H}^+ + 2e$	$\sigma_e^{\text{doub. ion.}}$	§3.2
$p_{\text{CR}} + \text{He} \rightarrow p_{\text{CR}} + \text{He}^+ + e$	$\sigma_p^{\text{ion.}}$	§4.1
$p_{\text{CR}} + \text{He} \rightarrow \text{H} + \text{He}^+$	$\sigma_p^{\text{e. c.}}$	§4.2
$e_{\text{CR}} + \text{He} \rightarrow e_{\text{CR}} + \text{He}^+ + e$	$\sigma_e^{\text{ion.}}$	§4.3

ization rate in diffuse and dense clouds; finally, in Sect. 9 we summarize our conclusions.

2. CR reactions with H_2

CR particles (electrons, protons, and heavy nuclei) impact with atoms and molecules of the ISM producing ions and electrons. Table 1 lists the main CR ionization reactions involving H_2 and He. In molecular clouds, a large majority of CR– H_2 impacts leads to the formation of H_2^+ via the *ionization* reaction



where k_{CR} is a cosmic-ray particle of species k and energy E_k , with cross section $\sigma_k^{\text{ion.}}$. Here we consider CR electrons ($k = e$), protons ($k = p$), and heavy nuclei of charge Ze ($k = Z$, with $Z \geq 2$). Low-energy CR protons, in addition, may react with ambient H_2 by *electron capture* reactions,



with cross section $\sigma_p^{\text{e. c.}}$. For an isotropic distribution of CR particles, the production rate of H_2^+ (per H_2 molecule) is then

$$\zeta^{\text{H}_2} = 4\pi \sum_k \int_{I(\text{H}_2)}^{E_{\text{max}}} j_k(E_k) [1 + \phi_k(E_k)] \sigma_k^{\text{ion.}}(E_k) E_k + 4\pi \int_0^{E_{\text{max}}} j_p(E) \sigma_p^{\text{e. c.}}(E_p) E_p, \quad (3)$$

where $j_k(E_k)$ is the number of CR particles of species k per unit area, time, solid angle and per energy interval (hereafter, we will refer to $j_k(E_k)$ simply as the spectrum of particle k), $I(\text{H}_2) = 15.603 \text{ eV}$ is the ionization potential of H_2 , and $E_{\text{max}} = 10 \text{ GeV}$ is the maximum energy considered. The quantity $\phi_k(E_k)$ is a correction factor accounting for the ionization of H_2 by secondary electrons. In fact, secondary electrons are sufficiently energetic to induce further ionizations of H_2 molecules, and their relatively short range justifies a local treatment of their ionizing effects. The number of secondary ionization produced per primary ionization of H_2 by a particle k is determined by

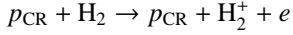
$$\phi_k(E_k) \equiv \frac{1}{\sigma_k^{\text{ion.}}(E_k)} \int_{I(\text{H}_2)}^{E'_{\text{max}}} P(E_k, E'_e) \sigma_e^{\text{ion.}}(E'_e) E'_e, \quad (4)$$

where $P(E_k, E'_e)$ is the probability that a secondary electron of energy E'_e is ejected in a primary ionization by a particle of energy E_k . The spectrum of secondary electrons declines rapidly with E'_e from the maximum at $E'_e = 0$ (Glassgold & Langer 1973b; Cecchi-Pestellini & Aiello 1992). The function

$\phi_e(E_e)$ giving the number of secondary ionizations after a single ionization by an electron of energy E_e has been computed by Glassgold & Langer (1973b) for energies of the incident electron up to 10 keV. Above a few 100 eV, ϕ_e increases logarithmically with E_e . For secondary electrons produced by impact of particles k , we adopt the scaling $\phi_k(E_k) \approx \phi_e(E_e = m_e E_k/m_k)$ valid in the Bethe-Born approximation. Calculations by Cravens & Dalgarno (1978) confirm this scaling for protons in the range 1–100 MeV.

In the following subsections we summarize the available data for the ionization cross sections for proton and electron impact and for the electron capture cross section. The ionization of H_2 by CR heavy-nuclei ($Z \geq 2$) is computed in the Bethe-Born approximation as described in Appendix A.

2.1. Ionization of H_2 by proton impact:



The available experimental data for proton-impact ionization of H_2 have been summarized by Rudd et al. (1985). The cross section has a maximum at $E_p \approx 70$ keV and is considerably uncertain below ~ 1 keV. The data were fitted by Rudd et al. (1985) with expressions appropriate to the high- and low-energy regions,

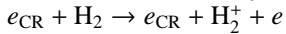
$$\sigma_p^{\text{ion.}} = (\sigma_l^{-1} + \sigma_h^{-1})^{-1}, \quad (5)$$

where

$$\sigma_l = 4\pi a_0^2 C x^D, \quad \sigma_h = 4\pi a_0^2 [A \ln(1+x) + B] x^{-1}, \quad (6)$$

with $x = m_e E_p/m_p I(H)$, $I(H) = 13.598$ eV, $A = 0.71$, $B = 1.63$, $C = 0.51$, $D = 1.24$. This expression is compared with experimental data in Fig. 1. For comparison, we also show in Fig. 1 the Bethe (1933) cross section for primary ionization of atomic hydrogen multiplied by a factor of 2. As it is evident, the Bethe formula reproduces very well the behavior of the ionization cross section at energies above a few tens of MeV.

2.2. Ionization of H_2 by electron impact:



The experimental data for electron-impact ionization of H_2 have been reviewed by Liu & Shemansky (2004). The absolute cross sections for electron-impact ionization of H_2 measured by Straub et al. (1996) in the energy range $E_e = 17$ eV to $E_e = 1$ keV represent the currently recommended experimental values (Lindsay & Mangan 2003). Analytic expressions and fitting formulae for the ionization cross section have been derived by Rudd (1991), Kim & Rudd (1994) and Liu & Shemansky (2004). Here we adopt the semi-empirical model by Rudd (1991) that gives an analytical expression valid up to relativistic velocities based on the theoretical results of Mott (1930),

$$\sigma_e^{\text{ion.}} = 4\pi a_0^2 N \left[\frac{I(H)}{I(H_2)} \right]^2 F(t)G(t), \quad (7)$$

where $t = E_e/I(H_2)$, $N = 2$ (number of electrons of H_2),

$$F(t) = \frac{1-t^{1-n}}{n-1} - \left(\frac{2}{1+t} \right)^{n/2} \frac{1-t^{1-n/2}}{n-2}, \quad (8)$$

$$G(t) = \frac{1}{t} \left(A_1 \ln t + A_2 + \frac{A_3}{t} \right), \quad (9)$$

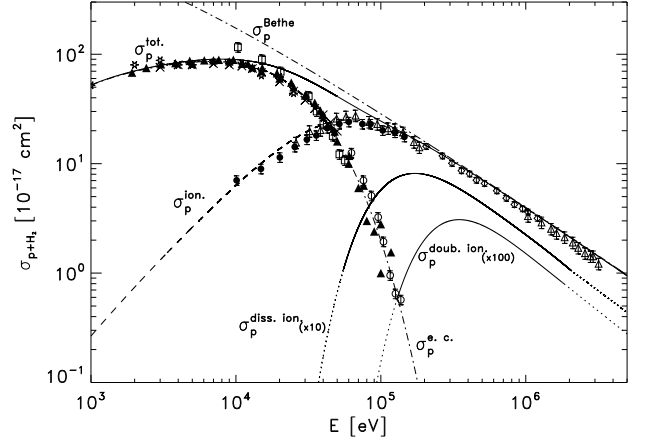
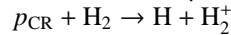


Fig. 1. Cross sections for proton impact on H_2 : ionization cross section $\sigma_p^{\text{ion.}}$ (Rudd et al. 1985) and electron capture $\sigma_p^{\text{e. c.}}$ (Rudd et al. 1983) and total cross section $\sigma_p^{\text{tot.}}$ for production of H_2^+ . For comparison, the *dot-dashed line* shows the Bethe ionization cross section multiplied by a factor of 2. The two lower curves show the cross sections for dissociative ionization and double ionization of H_2 , multiplied by a factor of 10 and 100, respectively, obtained from the corresponding expressions for electron impact at equal velocity. Experimental data for the ionization cross section: *stars*, Gilbody & Hasted (1957); *triangles*, Afrosimov et al. (1958); *diamonds*, Hooper et al. (1961); *filled circles*, deHeer, Schutten & Moustafa (1966); Experimental data for the electron capture cross section: *crosses*, Curran, Donahue & Kasner (1959); *empty circles*, deHeer, Schutten & Moustafa (1966); *asterisks*, McClure (1966); *squares*, Toburen & Wilson (1972).

with $n = 2.4 \pm 0.2$, $A_1 = 0.74 \pm 0.02$, $A_2 = 0.87 \pm 0.05$, $A_3 = -0.60 \pm 0.05$. For comparison, we also show in Fig. 2 the Bethe (1933) cross section for primary ionization of atomic hydrogen multiplied by a factor of 2. The Bethe formula reproduces very well the behavior of the ionization cross section at energies above a few tens of keV.

2.3. Electron capture ionization of H_2 :



In this charge-exchange process, a high-energy CR proton picks up an electron from the H_2 molecule and emerges as a neutral H atom. The electron capture cross section has been fit by Rudd et al. (1983) with the expression

$$\sigma_p^{\text{e. c.}} = 4\pi a_0^2 AN \left[\frac{I(H)}{I(H_2)} \right]^2 \frac{x^2}{C + x^B + Dx^F}, \quad (10)$$

where $x = E_p/I(H)$, $N = 2$ (number of electrons of H_2), $A = 1.044$, $B = 2.88$, $C = 0.016$, $D = 0.136$, $F = 5.86$. This expression is compared in Fig. 1 with available experimental results.

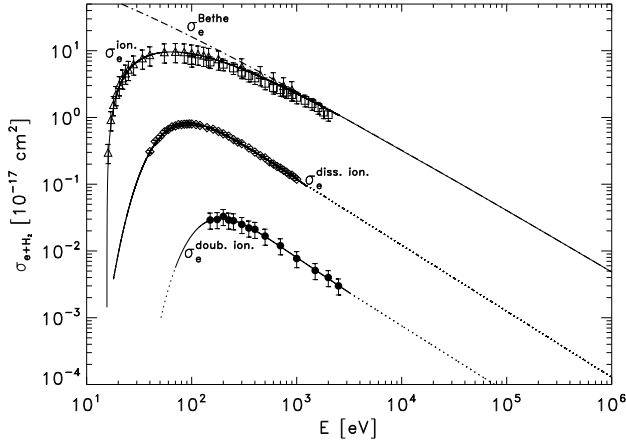
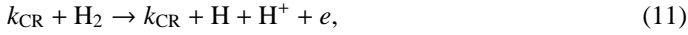


Fig. 2. Cross sections for electron impact on H_2 : ionization cross section $\sigma_p^{\text{ion.}}$ (Rudd 1991), dissociative ionization $\sigma_p^{\text{diss.ion.}}$, and double ionization cross section $\sigma_p^{\text{doub.ion.}}$ (polynomial fits of Table 2, *solid* part of the curves). For comparison, the *dot-dashed* line shows the Bethe ionization cross section multiplied by a factor of 2. Experimental data for the ionization cross section: *triangles*, Rapp & Englander-Golden (1965); *squares*, Kossmann, Schwarzkopf & Schmidt (1990). Experimental data for the dissociative ionization cross section: *diamonds*, Straub et al. (1996). Experimental data for the double ionization cross section: *filled circles*, Kossmann, Schwarzkopf & Schmidt (1990).

3. Additional reactions of CR electrons and protons with H_2

Additional ionization reactions that produce electrons are the *dissociative ionization* of H_2 ,



with cross section $\sigma_k^{\text{diss. ion.}}$, and the *double ionization* of H_2 ,



with cross section $\sigma_k^{\text{doub. ion.}}$. These two processes contribute to the total CR production rate of electrons per H_2 molecule,

$$\begin{aligned} \zeta^e = & 4\pi \sum_k \int_{I(\text{H}_2)}^{E_{\text{max}}} j_k(E_k) [1 + \phi_k(E_k)] \sigma_k^{\text{ion.}}(E_k) dE_k \\ & + 4\pi \sum_k \int_{E_{\text{diss. ion.}}}^{E_{\text{max}}} j_k(E) [1 + \phi_k(E)] \sigma_k^{\text{diss. ion.}}(E) dE \\ & + 8\pi \sum_k \int_{E_{\text{doub. ion.}}}^{E_{\text{max}}} j_k(E) [1 + \phi_k(E)] \sigma_k^{\text{doub. ion.}}(E) dE. \quad (13) \end{aligned}$$

In the following subsection we examine the cross sections of these two processes for electron impact reactions, whereas for proton impact we assume cross sections equal to the corresponding cross sections for electrons of equal velocity,

$$\sigma_p^{\text{diss. ion.}}(E_p) = \sigma_e^{\text{diss. ion.}}(E_e = m_e E_p / m_p) \quad (14)$$

and

$$\sigma_p^{\text{doub. ion.}}(E_p) = \sigma_e^{\text{doub. ion.}}(E_e = m_e E_p / m_p). \quad (15)$$

Table 2. Fit coefficients for the dissociative ionization and double ionization cross sections of H_2 by electron impact. The cross sections are given by $\log(\sigma_e / 10^{-18} \text{ cm}^2) = \sum_n a_n \log(E_e / \text{eV})^n$.

n	a_n (diss. ion.)	a_n (doub. ion.)
0	-53.23133	-125.8689
1	96.57789	172.0709
2	-67.57069	-108.8777
3	23.32707	34.18291
4	-4.004618	-5.358045
5	0.272652	0.335476

As shown below, the cross sections of these processes are smaller by at least one order of magnitude than the corresponding ionization cross section, and the relative contribution of dissociative ionization and double ionization to the total electron production rate is expected to be small.

3.1. Dissociative ionization of H_2 by electron impact:



Absolute partial cross sections for dissociative ionization of H_2 by electron impact (threshold $E_e^{\text{diss. ion.}} = 18.1 \text{ eV}$) have been measured by Straub et al. (1996) for incident electron energies ranging from $E_e = 25 \text{ eV}$ to $E_e = 1 \text{ keV}$ (see also Lindsay & Mangan 2003). Their results are in agreement with the reanalysis of Van Zyl & Stephen (1994) of the experimental results of Rapp, Englander-Golden & Briglia (1965), Krishnakumar & Srivastava (1994). For $1 \text{ keV} < E_e < 6 \text{ keV}$, the cross section has been measured by Takayanagi & Suzuki (1978). These measurements represent the currently recommended experimental values (Liu & Shemansky 2004). The data of Straub et al. (1996) and a polynomial fit of the data are shown in Fig. 2. The coefficients of the polynomial fit, valid for $18.1 \text{ eV} < E_e < 2 \text{ keV}$, are given in Table 2.

3.2. Double ionization of H_2 by electron impact:



The energy threshold for this reaction is $E_e^{\text{doub. ion.}} = 51 \text{ eV}$. The cross section for this reaction is highly uncertain: the measurements by Edwards et al. (1988) and Kossmann, Schwarzkopf & Schmidt (1990) disagree by a factor of ~ 8 . Here we adopt the latter set of measurements (shown in Fig. 2). The coefficients of a polynomial fit of these data, valid for $51 \text{ eV} < E_e < 4 \text{ keV}$, are given in Table 2.

4. CR reactions with He

The CR production rate of He^+ (per He atom) is

$$\begin{aligned} \zeta^{\text{He}} = & 4\pi \sum_k \int_{I(\text{He})}^{E_{\text{max}}} j_k(E_k) [1 + \phi_k(E_k)] \sigma_k^{\text{ion.}}(E_k) dE_k \\ & + 4\pi \int_0^{E_{\text{max}}} j_p(E) \sigma_p^{e. c.}(E_p) dE_p. \quad (16) \end{aligned}$$

where $I(\text{He}) = 24.587 \text{ eV}$ is the ionization potential of He, $\sigma_k^{\text{ion.}}$ is the ionization cross sections of He for impact by particles k , and $\sigma_p^{e. c.}$ is the electron capture cross section. In the following subsections we describe the relevant cross section data proton and electron impact on He. As in the case of H_2 , the ionization

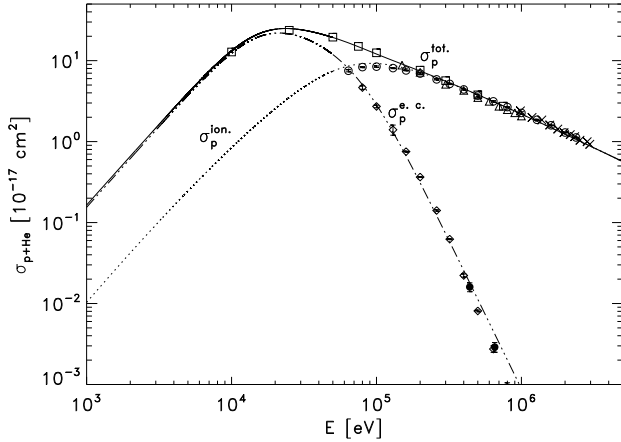
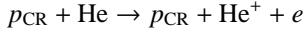


Fig. 3. Cross sections for proton impact on He: ionization cross section σ_p^{ion} (Rudd et al. 1983), electron capture cross section $\sigma_p^{\text{e.c.}}$, and total cross section σ_p^{tot} for production of He^+ . Experimental data for the ionization cross section: circles, Shah & Gilbody (1985). Data for the electron capture cross section: *filled circles*, Welsh et al. (1967); *diamonds*, Shah & Gilbody (1985). Data for the total ionization cross section: crosses, Pivovar & Levchenko (1967); *triangles*, Puckett & Martin (1970); squares, DuBois, Toburen & Rudd (1984).

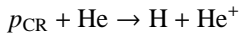
of He by CR heavy-nuclei is computed in the Bethe-Born approximation described in Appendix A.

4.1. Ionization of He by proton impact:



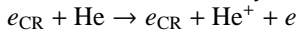
Experimental measurements of He ionization by proton impact have been collected and fitted by Rudd et al. (1985). The cross section has a maximum at $E_p \approx 100$ keV and is considerably uncertain below ~ 10 keV. Fig. 3 shows the available experimental data. We adopt the fitting formula of Rudd et al. (1985) given by eq. (5) and (6) with parameters $A = 0.49$, $B = 0.62$, $C = 0.13$, $D = 1.52$.

4.2. Ionization of He by electron capture:



The cross section for this charge transfer reaction has been measured by Welsh et al. (1967) and Shah & Gilbody (1985). The cross section has a maximum at $E_p \approx 25$ keV, where it is about one order of magnitude larger than the ionization cross section σ_p^{ion} . (see Fig. 3). Total ionization cross sections ($\sigma_p^{\text{ion}} + \sigma_p^{\text{e.c.}}$) have been reported by DuBois, Toburen & Rudd (1984).

4.3. Ionization of He by electron impact:



Accurate experimental measurements of the cross section of ionization of He by electron impact are available (see Fig. 4) and are in good agreement with theoretical calculations (Pindzola & Robicheaux 2000; Colgan et al. 2006). Here we adopt the fitting formula of Rudd (1991) given in eq. (7)–(9) with $N = 2$, $n = 2.4 \pm 0.3$, $A_1 = 0.85 \pm 0.04$, $A_2 = 0.36 \pm 0.09$, and $A_3 = -0.10 \pm 0.10$.

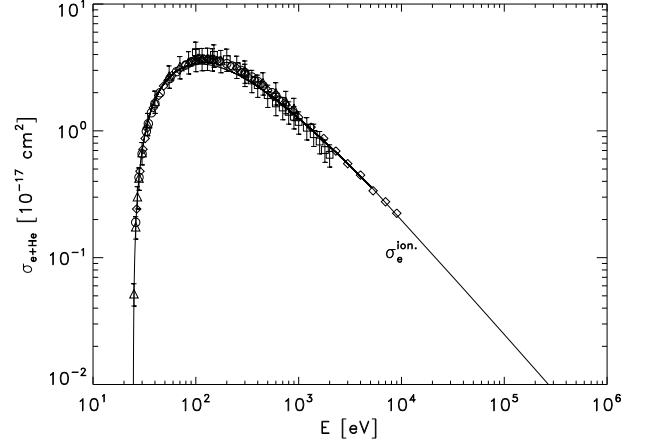


Fig. 4. Cross section for He ionization by electron impact σ_e^{ion} (Rudd 1991). Experimental data: *triangles*, Rapp & Englander-Golden (1965); *circles* Montague, Harrison, & Smith (1984); *diamonds*, Shah et al. (1988); *squares*, Kossmann, Schwarzkopf & Schmidt (1990).

5. Local interstellar spectra

From a theoretical point of view, if one assumes a uniform distribution (in space and time) of CR sources characterized by a given “source spectrum” (usually a power-law in rigidity), CR propagation models can generate steady-state local interstellar (LIS) spectra resulting from a number of processes affecting the CR transport in the Galactic disk, like nuclear interactions, ionization energy loss, radioactive decay, escape from the Galaxy, etc. (see e.g. Berezhinsky et al. 1990). These LIS spectra, in turn, can be used as input for solar modulation calculations to reproduce the CR spectrum and the relative abundances of CR particles measured at the Earth. The LIS spectra obtained in this way are clearly not uniquely defined, and a considerable range of LIS spectral shapes can be shown to be consistent with the measured CR flux with appropriate choices of parameters of the transport model (see e.g. Mewaldt et al. 2004, especially their Fig. 1).

It is generally assumed that the LIS spectrum characterizes the energy distribution of CR everywhere in the Galactic disk, as long as the ISM properties do not depart from the uniform conditions assumed in the propagation model. With this assumption, Webber (1998) adopted LIS spectra for protons and heavy nuclei of energy greater than 10 MeV and electrons of energy greater than 2 MeV and combined them with data from *Voyager* and *Pioneer* spacecraft measurements out to 60 AU from the Sun to obtain a CR ionization rate $\zeta^{\text{H}} \approx 3\text{--}4 \times 10^{-17} \text{ s}^{-1}$. This is 5–6 times the “standard” rate of Spitzer & Tomasko (1968) for atomic hydrogen.

It is very uncertain, however, whether LIS spectra are really representative of the whole galactic disk, especially because the Solar System resides in a low-density ($n \approx 10^{-3} \text{ cm}^{-3}$) region produced by ~ 10 supernovae exploded over the past 10 Myr (the “Local Bubble”). In addition, to compute reliable CR ionization rates, the demodulated spectra need to be extrapolated down to \sim keV energies where the ionization cross sections have a maximum (see Sect. 2, 3 and 4). Given these uncertainties, we discuss in the remainder of the paper the consequences for the CR ionization rate of making different assumptions about the low-energy behavior of CR spectra. In particular, we consider

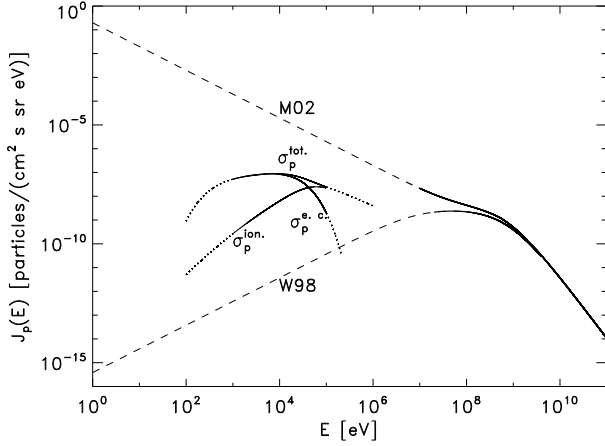


Fig. 5. Proton LIS spectra of M02 and W98 (upper and lower solid curves, respectively). The dashed curves represent our power-law extrapolations of the spectra. For comparison, the cross sections for ionization of H_2 by proton impact, electrons capture, and total ionization are also shown (in arbitrary units).

for both protons and electrons a “minimum” and “maximum” LIS spectrum compatible with the available observational constraints, and we compute the resulting ionization rates with the objective of comparing them with existing data for diffuse and dense clouds.

5.1. Proton local interstellar spectrum

We consider two determinations of the proton LIS spectrum: Webber (1998, “minimum”) and Moskalenko et al. (2002, “maximum”), labeled respectively W98 and M02. Their characteristics are the following.

(i) W98 estimated the LIS proton spectrum down to ~ 10 MeV, starting from an injection spectrum parametrized as a power-law in rigidity, propagated according to the model of Webber (1987) and accounting for solar modulation following Potgieter (1995). The effects of solar modulation were refined using data from the Voyager and Pioneer spacecraft, then at distances of ~ 60 – 70 AU from the Sun. The predicted LIS proton spectrum of W98 has a turnover around $E \approx 100$ MeV because of the dominant effect of ionization losses at low energies in the Galactic propagation model. Our extrapolation at low energies is a power-law in energy with exponent 0.95.

(ii) The adopted LIS spectrum of M02 (their “best-fitting” case) reproduces the observed spectrum of protons, antiprotons, alphas, the B/C ratio and the diffuse γ -ray background. It is obtained from an injection spectrum which is a double power-law in rigidity with a steepening below 20 GeV, and a flattening of the diffusion coefficient below 4 GeV to match the B/C ratio at $E \lesssim 100$ MeV. At low energies, our extrapolation follows a power-law in energy with exponent -1 .

Fig. 5 shows a comparison of the proton spectrum according to W98 and M02 (thick lines). The two spectra have been extrapolated as power laws down to \sim keV energies where the total ionization cross section, also shown in Fig. 5, has a broad maximum.

5.2. Electron local interstellar spectrum

CR electrons (and positrons), although constituting a small percentage of the corpuscular radiation, provide important information regarding interstellar propagation. This happens because CR electrons are more sensitive probes of ISM conditions than CR nuclei. In fact, electrons interact with: (i) the ISM, producing bremsstrahlung responsible for the largest part of galactic background at γ -frequencies; (ii) radiation fields, generating radiation by inverse Compton scattering at X- and γ -frequencies; (iii) magnetic fields, producing synchrotron emission at radio frequencies. The electromagnetic radiation emitted by the interaction of CR electrons with other components of the ISM makes it possible to establish a relation between the observed radiation spectra and the energy distribution of the electrons. In particular, observations of the γ -ray background in the 10 keV–100 MeV range, combined with measurements of the Galactic synchrotron spectral index in the frequency range 10 MHz–10 GHz, provide indirect constraints on the LIS electron spectrum down to energies of ~ 100 MeV. As for the proton spectrum, we extrapolate the LIS electron spectra to lower energies with power-laws to reach the peak of the ionization cross section at ~ 0.1 keV. Here we consider two different estimates of the LIS electron spectrum, both derived by Strong, Moskalenko & Reimer (2000).

(i) The first spectrum, labeled C00, corresponds to the “conventional” model C of Strong et al. (2000), and is mostly derived from radio observations. It reproduces the spectrum of electrons, protons and alphas above ~ 10 GeV, satisfies the limits imposed by positrons and antiprotons and the constraints on the synchrotron spectrum, but fails to account for the γ -ray background, especially for photon energies below ~ 30 MeV and above ~ 1 GeV. At low-energies, we have adopted a power-law dependence of the electron spectrum as $E_e^{0.08}$.

(ii) The second spectrum, labeled E00, corresponds to model E00 of Strong et al. (2000). It reproduces the γ observations at photon energies below ~ 30 MeV by a combination of bremsstrahlung and inverse Compton emission, assuming a steepening of the electron spectrum below ~ 200 MeV to compensate for the growth of ionization losses. The resulting increase in the synchrotron spectrum occurs at frequencies below 10 MHz, where the radio spectrum decreases abruptly due to the onset of free-free absorption. To fit OSSE data would require a LIS electron even steeper than E00, but the excess γ emission at \sim MeV energies may be due to a population of unresolved point sources (Strong et al. 2000). At low energies, we have adopted a power-law extrapolation of the spectrum as E_e^{-1} .

In Fig. 6 we compare the two LIS electron spectra E00 and C00 assumed in this work.

5.3. CR ionization rate for the local interstellar spectra

The values of $\zeta_k^{\text{H}_2}$, ζ_k^e and ζ_k^{He} per H_2 molecule and He atom, respectively, obtained from numerical integration of eq. (3), (13) and (16), with the $j_k(E_k)$ taken to be the adopted LIS spectra, are listed in Tab. 3. We have assumed a mixture of H_2 and He with $f_{\text{H}_2} = 0.83$ and $f_{\text{He}} = 0.17$, corresponding to a He/H ratio of 0.1. We also list in Table 3 the energy density of each CR component, defined as

$$\mathcal{E}_k = 4\pi \int_0^\infty \frac{j_k(E_k) E_k}{v_k(E_k)} dE_k \quad (17)$$

where $j_k(E_k)$ is the particle’s LIS spectrum and $v_k(E_k) = c(E_k^2/m_k^2 c^4 + 2E_k/m_k c^2)^{1/2}/(1 + E_k/m_k c^2)$ is the velocity of particle k with kinetic energy E_k . We compute the total energy density

of CR as $\sum_k \mathcal{E}_k \approx (1 + \xi) \mathcal{E}_p$, where $\xi = 0.41$ is the correction factor for the abundance of He and heavy nuclei (see Appendix A). The results listed in Table 3 suggest the following considerations:

(i) Protons and heavy nuclei (plus secondary electrons) can produce ionization rates ranging from $\sim 10^{-17} \text{ s}^{-1}$ (in the case of the spectrum W98, decreasing below $E_p \approx 100 \text{ MeV}$) to $\sim 10^{-14} \text{ s}^{-1}$ (spectrum M02, increasing below $E_p \approx 100 \text{ MeV}$). The contribution of CR electrons to the ionization rate is negligible if the LIS electron spectrum flattens below $E_e \approx 10 \text{ MeV}$ (spectrum C00), but can become dominant if the spectrum increases at low energies. In practice, the ionization rate is proportional to the flux of CR particles in the energy range where the contribution to the integrals in eq. (3), (13) and (16) is larger (see Sect. 7 and Fig. 14).

(ii) The ratio of the CR ionization rate of He and H_2 depends on the shape and absolute value of the assumed spectra. For CR protons, the ratio $\zeta_p^{\text{He}}/\zeta_p^{\text{H}_2}$ varies between 0.15 (spectrum M02) and 0.64 (spectrum W98), whereas for electrons it varies between 0.38 (spectrum E00) and 0.65 (spectrum C00). In general, since the ionization cross section for He decreases faster than that of H_2 below the maximum, CR spectra rising with decreasing energy result in a lower value of $\zeta^{\text{He}}/\zeta^{\text{H}_2}$. Given the sensitivity of modeled steady-state abundances of species like C, O_2 , H_2O , H_3^+ in dense clouds to the value of $\zeta^{\text{He}}/\zeta^{\text{H}_2}$ (Wakelam et al. 2006), it might be possible to constrain this ratio from a careful combination of molecular line observations and chemical model predictions.

(iii) As anticipated, the CR production rate of electrons in molecular clouds ζ_k^e is dominated by the CR ionization of H_2 (Sect. 2) and He (Sect. 4). The contributions of dissociative ionization and double ionization to ζ_k^e are small, about 5.5% and 0.32% of the rate of production of electrons by single ionization of H_2 , respectively, independent of the adopted spectrum.

(iv) The production rate of electrons, ζ_k^e , is generally larger than (but close to) the production rate of H_2^+ . For the W98 proton spectrum, the C00 and E00 electron spectra, $\zeta_k^{\text{H}_2} \approx 0.83\text{--}0.87\zeta_k^e$. However, since we have included in the expression for ζ^{H_2} the electron capture reaction (2) whose cross section peaks at a lower energy than the ionization reaction (1) as shown in Fig. 1, a CR proton spectrum rising at low energies may result in $\zeta_p^{\text{H}_2} > \zeta_p^e$, as in the case of the M02 spectrum.

(v) With our assumed LIS spectra, the total CR energy density varies from a minimum of 0.970 eV cm^{-3} (W98 plus C00) and a maximum of 1.80 eV cm^{-3} (M02 plus E00), corresponding to an equipartition magnetic field of $6.2 \mu\text{G}$ and $8.5 \mu\text{G}$, respectively. These equipartition values are compatible with the “standard” value of the magnetic field of $6.0 \pm 1.8 \mu\text{G}$ in the cold neutral medium of the Galaxy (Heiles & Troland 2005). They have interesting consequences for the location of the solar wind termination shock (see discussion in Webber 1998).

It is important to stress that the CR ionization rates listed in Table 3 have been obtained by integrating the spectra and the cross sections down to the ionization threshold of H_2 and He, and they must therefore be considered as upper limits on the ionization rate. This is especially true for the electron spectrum E00, which results in ionization rates exceeding the observed values by more than three orders of magnitude (see Sect. 8). In the past, LIS spectra have been used to compute the CR ionization rate in the ISM assuming an appropriate lower cut-off in the CR energy (e.g. Nath & Biermann 1994; Webber 1998). In this work, we use the LIS spectra to define the energy distribution of CR particles incident on the surface of the cloud. As we show in

Table 3. CR ionization rates $\zeta_k^{\text{H}_2}$ and ζ_k^{He} (per H_2 and per He, respectively), electron production rate ζ_k^e , and energy densities \mathcal{E}_k of CR protons (p) and electrons (e) for the LIS spectra assumed in this work. The proton ionization rates include the contribution of heavy nuclei.

k	ref.	$\zeta_k^{\text{H}_2}$ (s^{-1})	ζ_k^{He} (s^{-1})	ζ_k^e (s^{-1})	\mathcal{E}_k (eV cm^{-3})
p	W98	2.08×10^{-17}	1.33×10^{-17}	2.50×10^{-17}	0.953
p	M02	1.48×10^{-14}	2.16×10^{-15}	3.49×10^{-15}	1.23
e	C00	1.62×10^{-19}	1.05×10^{-19}	1.94×10^{-19}	0.0167
e	E00	6.53×10^{-12}	2.46×10^{-12}	7.45×10^{-12}	0.571

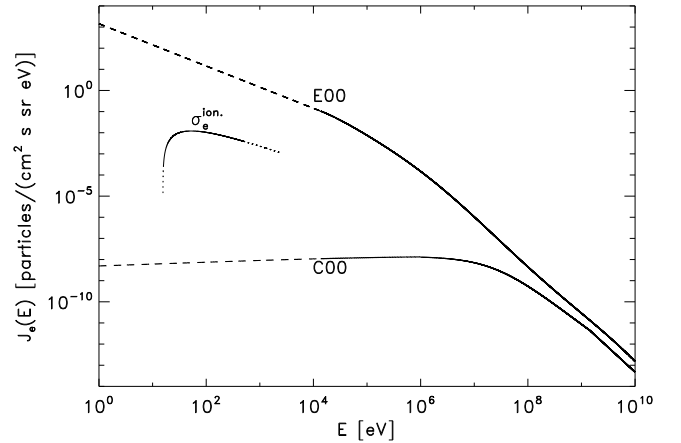


Fig. 6. Electron LIS spectra of E00 and C00 (upper and lower solid curves, respectively). The dashed curves represent our extrapolations of the spectra. For comparison, the cross section for ionization section of H_2 by electron impact is also shown (in arbitrary units).

Sect. 6 and 7, the low-energy tail of the CR spectrum is strongly (and rapidly) modified by various energy loss processes when the particles propagate in a medium denser than the local ISM.

6. Energy losses of CRs in the ISM

The penetration of primary CR and secondary particles in interstellar clouds was studied by Takayanagi (1973) and more in detail by Umebayashi & Nakano (1981). In this paper we adopt the LIS spectra discussed in Sect. 5 to characterize the incident spectra and we follow the propagation of CR particles inside a molecular cloud with the so-called *continuous-slowing-down approximation* (hereafter CSDA)¹. In this approximation, the “degradation spectrum” of the CR component k resulting from the energy loss of the incident particles and the generation of

¹ In the astrophysical literature this approximation is often referred to as the *continuous energy loss regime*, and when the propagation is dominated by these losses, it is often known as the *thick target approximation* (see e.g. Ramaty & Lingenfelter 1975; Ramaty, Kozlovsky & Lingenfelter 1996).

secondary particles is proportional to the inverse of the *energy loss function*, defined by

$$L_k(E_k) = -\frac{1}{n(\text{H}_2)} \left(\frac{dE_k}{d\ell} \right), \quad (18)$$

where $n(\text{H}_2)$ is the density of the medium in which the particles propagate and ℓ is the path length. Since we consider only energy losses in collisions with H_2 , our results are applicable only to clouds in which hydrogen is mostly in molecular form.

In the following we consider CR propagation in molecular clouds assuming a plane-parallel geometry. It is convenient to introduce the column density of molecular hydrogen $N(\text{H}_2)$,

$$N(\text{H}_2) = \int n(\text{H}_2) d\ell, \quad (19)$$

and to rewrite the energy loss function (eq. 18) as

$$L_k(E_k) = -\frac{dE_k}{dN(\text{H}_2)}. \quad (20)$$

Let us then define $j_k(E_k, N)$ as the spectrum of CR particles of species k at depth $N(\text{H}_2)$, with $j_k(E_k, 0)$ representing the LIS spectrum incident on the cloud's surface, defined by a column density $N(\text{H}_2) = 0$. To compute $j_k(E_k, N)$ we must consider all the processes that degrade the energy of the incident CR particles. Assuming that the direction of propagation does not change significantly inside the cloud, it follows from eq. (20) that particles of initial energy $E_{k,0}$ reach energy $E_k < E_{k,0}$ as a consequence of energy losses after propagating across a column density $N(\text{H}_2)$ given by

$$N(\text{H}_2) = -\int_{E_k}^{E_{k,0}} \frac{dE_k}{L_k(E_k)} = n(\text{H}_2)[R_k(E_{k,0}) - R_k(E_k)], \quad (21)$$

where $R_k(E_k)$ is the *range*, defined as

$$R_k(E_k) = \int_{E_k}^0 d\ell = \int_0^{E_k} \frac{dE_k}{-(dE_k/dx)} = \frac{1}{n(\text{H}_2)} \int_0^{E_k} \frac{dE_k}{L_k(E_k)}. \quad (22)$$

Conservation of the the number of CR particles of each species implies

$$j_k(E_k, N) dE_k = j_k(E_{k,0}, 0) dE_{k,0}, \quad (23)$$

where, for a given value of $N(\text{H}_2)$, the infinitesimal variation $dE_{k,0}$ of the particle's initial energy corresponds to an infinitesimal variation dE_k of its energy at a depth $N(\text{H}_2)$ given by

$$\frac{dE_k}{L_k(E_k)} = \frac{dE_{k,0}}{L_k(E_{k,0})} \quad (24)$$

(we ignore here that electron capture reactions of CR protons with H_2 and He do not conserve the number of CR protons). Thus, the relation between the incident spectrum $j_k(E_{k,0})$ and the spectrum at depth $j_k(E_k, N)$ in the CSDA is

$$j_k(E_k, N) = j_k(E_{k,0}) \frac{dE_k}{dE_{k,0}} = j_k(E_{k,0}) \frac{L_k(E_{k,0})}{L_k(E_k)}. \quad (25)$$

The energy loss functions for electrons and protons in H_2 are shown in Fig. 7. Some energy loss processes are common to CR protons and electrons, like Coulomb interactions, inelastic collisions and ionization; others are peculiar to protons (elastic collisions, pion production and spallation), others to electrons (bremsstrahlung, synchrotron emission and inverse Compton scattering). These processes are briefly reviewed in the following subsections.

6.1. Energy loss of protons colliding with H_2

To determine the energy loss function of protons we have used the results collected by Phelps (1990) for energies in the range from 10^{-1} eV to 10^4 eV. For higher energies, between 1 keV and 10 GeV, we have used data from the NIST Database² for atomic hydrogen multiplied by a factor of 2 to obtain the corresponding values for collisions with molecular hydrogen (NIST data do not include pion production at energies higher than about 0.5 GeV, that we computed following Schlickeiser 2002). The resulting energy loss function is shown in Fig. 7. The broad peak in $L_p(E_p)$ at $E_p \approx 10$ eV is due to elastic collisions and to the excitation of rotational and vibrational levels, the peak at $E_p \approx 100$ keV to ionization, and the rapid increase at energies above ~ 1 GeV is due to pion production. For the low ionization levels characteristic of molecular clouds, the energy loss for Coulomb interactions of CRs with ambient electrons can be neglected at energies above ~ 1 eV (dashed line in Fig. 7).

In Fig. 8 we show the quantity $n(\text{H}_2)R_p(E_p)$, obtained with a numerical integration of eq. (22), compared with data from the NIST Database at energies from 1 keV to 10 GeV. We also show the fit adopted by Takayanagi (1973) in a limited range of energies and the results of Cravens & Dalgarno (1978). As one can see, except for energies higher than ~ 100 MeV, where the NIST data do not include energy losses by pion production, the agreement between our results and the NIST data is very good.

6.2. Energy loss of electrons colliding with H_2

To determine the electron energy loss function we have adopted the results of Dalgarno et al. (1999) for 10^{-2} eV $\leq E_e \leq 1$ keV and those of Cravens, Victor & Dalgarno (1975) for 1 eV $\leq E_e \leq 10$ keV. For higher energies, 10 keV $\leq E_e \leq 10$ GeV, we have adopted the loss function for electron-H collisions from the NIST Database multiplied by a factor of 2. The resulting energy loss function is also shown in Fig. 7. The first peak in $L_e(E_e)$ is due to the excitation of vibrational levels, the second to the excitation of the electronic levels and ionization, while at higher energies the energy loss function is dominated by bremsstrahlung. As in the case of CR protons, we can neglect the contribution of Coulomb interactions for electrons at energies above ~ 1 eV. In Fig. 8, we show the range for electrons in H_2 , obtained as in the case of CR protons, compared with data from the NIST Database for 10 keV $\leq E_e \leq 1$ GeV.

7. CR ionization rate in diffuse and dense clouds

To compute the CR ionization rate in the ISM as a function of the column density $N(\text{H}_2)$ of traversed matter, we follow the method of Takayanagi (1973). First, varying E_k and $E_{k,0}$ from 0.1 eV to 100 GeV, we determine the column density from the difference between $R_k(E_{k,0})$ and $R_k(E_k)$. Second, tracing the level contours of the surface $N(E_{k,0}, E_k)$ at different values of $N(\text{H}_2)$, we obtain the relation between the energy of the incident CR particle, $E_{k,0}$, and the residual energy E_k , when the particle has covered a path inside the cloud corresponding to a given value of the column density. We then fit the resulting $E_{k,0}$ vs. E_k relation at fixed $N(\text{H}_2)$ with the expression

$$E_{k,0}(E_k, N) = \left(cE_k^b + \frac{N}{N_0} \right)^{1/b}, \quad (26)$$

² <http://physics.nist.gov/PhysRefData/Star/Text>

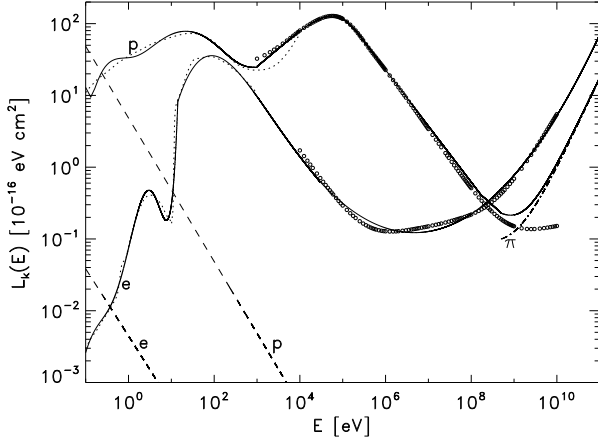


Fig. 7. Energy loss functions $L_e(E_e)$ and $L_p(E_p)$ for electrons and protons colliding with H_2 (solid curves), compared with NIST data (circles); dashed curves show Coulomb losses for a fractional electron abundance $n(e)/n(H_2) = 10^{-7}$; dash-dotted curves labelled with π represent the energy loss by pion production computed following Schlickeiser (2002); dotted curves show the results by Phelps (1990) and Dalgarno et al. (1999) for $p-H_2$ and $e-H_2$, respectively.

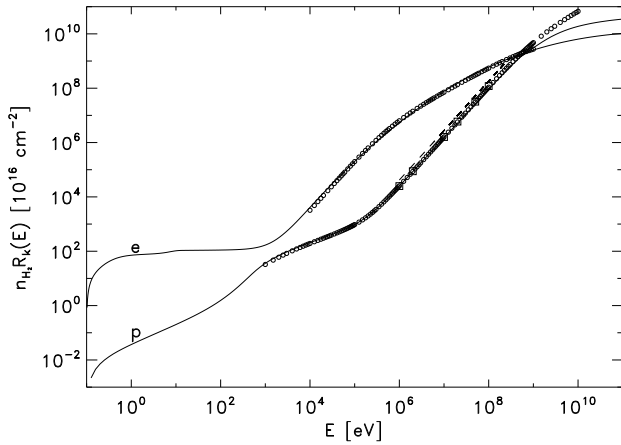


Fig. 8. Range $R_e(E_e)$ and $R_p(E_p)$ for electrons and protons colliding with H_2 (solid curves), compared with NIST data (circles) and the results of Cravens & Dalgarno (1978, squares); the dashed curve shows the fit by Takayanagi (1973)

where E_k and $E_{k,0}$ are in eV, N and N_0 in cm^{-2} , b and c are non-dimensional.

In Fig. 9, 10, 11, and 12 we show the CR spectrum obtained from eq. (25) and (26) for protons and electrons at values of $N(H_2)$ ranging from 10^{19} cm^{-2} to 10^{26} cm^{-2} , inside a molecular cloud for the two incident spectra of protons and electrons described in Sect. 5. One can notice the correspondence between the shape of the proton spectra shown in Fig. 9 and 10, and the energy loss function $L_p(E)$ shown in Fig. 7. In fact, the relative minimum at about 10 eV in the attenuated spectrum corresponds to the energy loss peak due to elastic interactions and excitation of roto-vibrational levels, and the minimum at about 100 keV

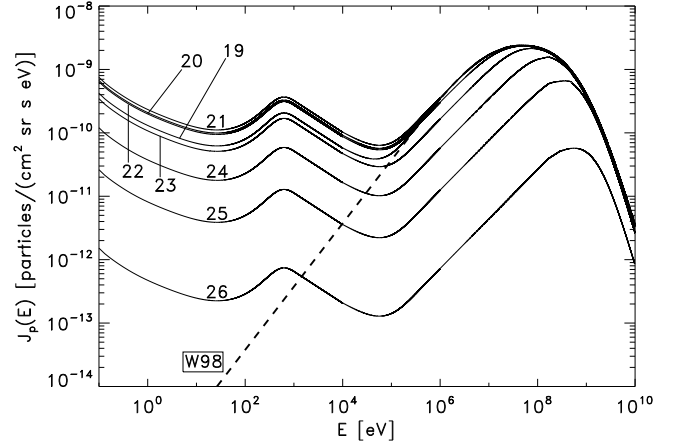


Fig. 9. Dashed curve: LIS proton spectrum W98 incident on the cloud's surface; dash-dotted curves: attenuated proton spectra at increasing depth in the cloud labeled by values of $\log[N(H_2)/\text{cm}^{-2}]$.

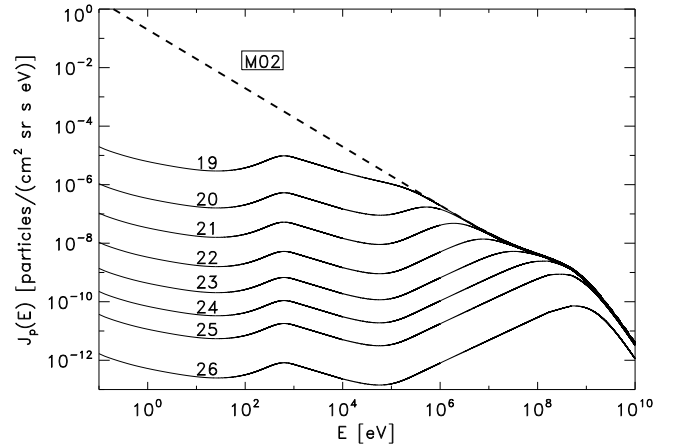


Fig. 10. Dashed curve: LIS proton spectrum M02 incident on the cloud's surface; dash-dotted curves: attenuated proton spectra at increasing depth in the cloud labeled by values of $\log[N(H_2)/\text{cm}^{-2}]$.

corresponds to the energy loss peak due to ionization. The same correspondence can be seen between electron spectra (Fig. 11 and 12) and the energy loss function $L_e(E_e)$ (Fig. 7): the minima in the spectrum at about 1 eV and 100 eV are caused by the energy loss due to the excitation of vibrational levels, and to the excitation of electronic levels and ionization, respectively. This is a well-known property of the CSDA, where one approximately obtains $j_k(E_k, N) \propto 1/L_k(E_k)$ independent on the column density if $N(H_2) \ll N_0$ (see eq. 26).

We are now able to calculate the CR ionization rate inside a molecular cloud as a function of the column density, with the attenuated spectra given by eq. (25). We compute the CR ionization rate for $N(H_2)$ between 10^{19} cm^{-2} and 10^{25} cm^{-2} , and we show the results for the four incident LIS spectra in Fig. 13.

As a result of the detailed treatment of CR propagation, the decrease of the ionization rate with increasing penetration in the

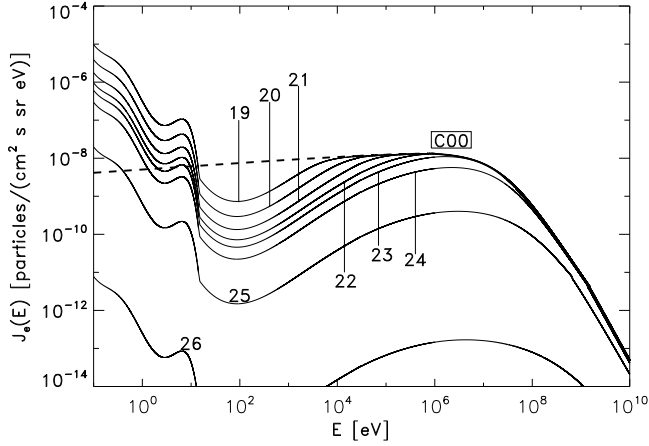


Fig. 11. Dashed curve: LIS electron spectrum C00 incident on the cloud’s surface; dash-dotted curves: attenuated proton spectra at increasing depth in the cloud labeled by values of $\log[N(\text{H}_2)/\text{cm}^{-2}]$.

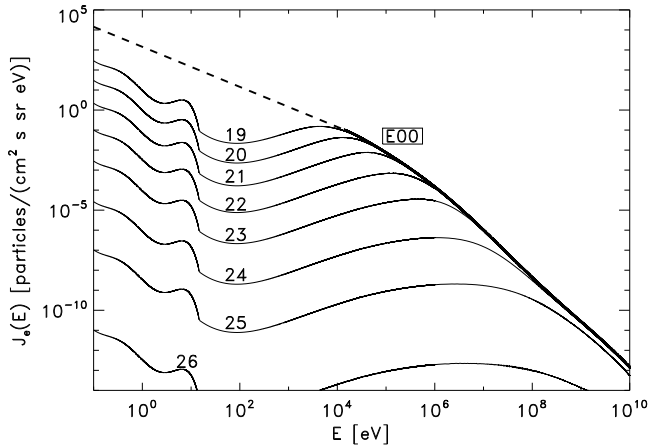


Fig. 12. Dashed curve: LIS electron spectrum E00 incident on the cloud’s surface; dash-dotted curves: attenuated proton spectra at increasing depth in the cloud labeled by values of $\log[N(\text{H}_2)/\text{cm}^{-2}]$.

cloud at column densities in the range $\sim 10^{20}$ – 10^{25} cm^{-2} is characterized by a power-law behavior, rather than exponential attenuation, and can be approximated as

$$\zeta_k^{\text{H}_2} \approx \zeta_{0,k} \left[\frac{N(\text{H}_2)}{10^{20} \text{ cm}^{-2}} \right]^{-a}. \quad (27)$$

We have fitted this expression to the numerical results shown in Fig. 13. The coefficients $\zeta_{0,k}$ and a are given in Table 4. The exponential attenuation of the CR ionization rate sets in for column densities larger than $\sim 10^{25}$ cm^{-2} , where $\zeta_k^{\text{H}_2}$ depends essentially on the flux of CR particles in the high-energy tail of the incident spectrum (above ~ 0.1 – 1 GeV), and directly measurable on the Earth. In this regime, the attenuation of the CR ionization rate is expressed as function of the surface density of traversed matter $\Sigma = \mu m_p N(\text{H}_2)$, where m_p is the proton mass and $\mu = 2.36$ is the molecular weight for the assumed fractional abundances of H_2

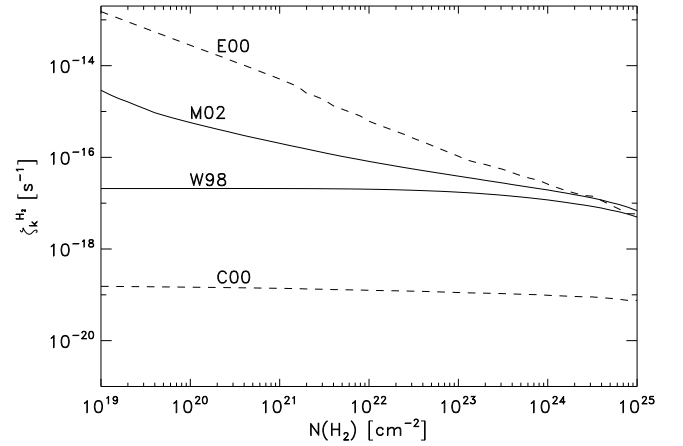


Fig. 13. CR ionization rate $\zeta_k^{\text{H}_2}$ as a function of the column density $N(\text{H}_2)$. Solid curves: contribution of CR protons (spectra W98 and M02); dashed curves, contribution of CR electrons (spectra C00 and E00).

Table 4. Fitting coefficients for eq. (27), describing the attenuation of the CR ionization rate for protons (p , also including heavy nuclei) and electrons (e). Eq. 27 is valid in the column density range $10^{20} \text{ cm}^{-2} \lesssim N(\text{H}_2) \lesssim 10^{25} \text{ cm}^{-2}$.

k	spectrum	$\zeta_{0,k}$ (s^{-1})	a
p	W98	2.0×10^{-17}	0.021
p	M02	6.8×10^{-16}	0.423
e	C00	1.4×10^{-19}	0.040
e	E00	2.6×10^{-14}	0.805

Table 5. Fitting coefficients for eq. (28) describing the attenuation of CR protons (p , also including heavy nuclei) and electrons (e). Eq. 28 is valid for $N(\text{H}_2) \gtrsim 10^{25} \text{ cm}^{-2}$.

k	spectrum	$\zeta_{0,k}$ (s^{-1})	$\Sigma_{0,k}$ (g cm^{-2})
p	W98	3.4×10^{-18}	44
p	M02	5.4×10^{-18}	38
e	C00	3.3×10^{-20}	71
e	E00	4.9×10^{-18}	35

and He ($f_{\text{H}_2} = 0.82$ and $f_{\text{He}} = 0.18$). For $\Sigma \gtrsim 1$ g cm^{-2} , we can fit the CR ionization rate as

$$\zeta_k^{\text{H}_2} \approx \zeta_{0,k} \exp\left(-\frac{\Sigma}{\Sigma_{0,k}}\right) \quad (28)$$

where $\Sigma_{0,k}$ is the attenuation surface density. In Table 5 we list the values of $\zeta_{0,k}$ and $\Sigma_{0,k}$ obtained with the four spectra considered in this work. The values for the attenuation surface density $\Sigma_{0,p}$ listed in Table 5 are significantly lower than the “standard” value of Nakano & Tademaru (1972) and Umebayashi & Nakano (1981), who obtain $\Sigma_{0,p} \simeq 96$ g cm^{-2} for $\Sigma \gtrsim 50$ g cm^{-2} (see also Umebayashi & Nakano 2009).

It is important to stress that a large contribution to the ionization of H_2 comes from low-energy protons and electrons constantly produced (in our steady-state model) by the slowing-

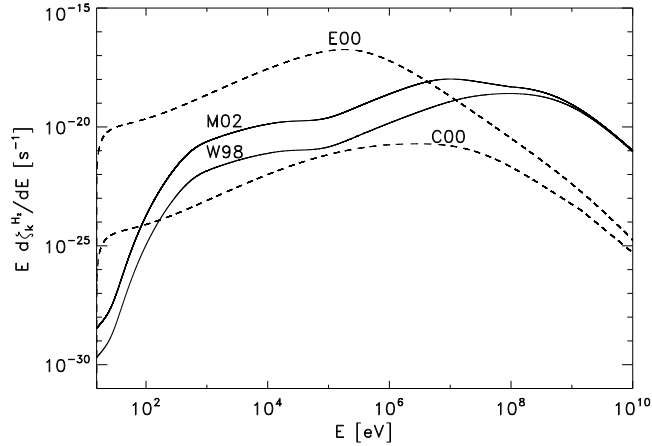


Fig. 14. Differential contribution to the ionization rate $E d\zeta_k^{\text{H}_2}/dE$ per logarithmic interval of kinetic energy, for the four spectra considered in this paper at a depth $N(\text{H}_2) = 10^{22} \text{ cm}^{-2}$ (solid curves, protons; dashed curves, electrons).

down of more energetic particles losing energy by interaction with the ambient H_2 . In Fig. 14 we show the differential contribution of CRs protons and electrons to the ionization rate at a depth of $N(\text{H}_2) = 10^{22} \text{ cm}^{-2}$, corresponding to the typical column density of a dense cloud. For protons and heavy nuclei, the bulk of the ionization is provided by CR in the range 1 MeV–1 GeV and by a “shoulder” in the range 1–100 keV produced by slowed-down protons. This low-energy tail is produced during the propagation of CR protons in the cloud even when the incident spectrum is devoid of low-energy particles (as shown in Fig. 9 for the W98 spectrum). The largest contribution of CR-electrons to the ionization is distributed over energies in the range 10 keV–10 MeV, again reflecting the distribution of electrons in the propagated spectra (see Fig. 11 and 12). Thus, the ionization rate at any depth in a cloud cannot be calculated by simply removing from the incident spectrum particles with energies corresponding to ranges below the assumed depth.

8. Comparison with observations

To obtain the total CR ionization rate in molecular clouds, we sum the ionization rates of protons (corrected for heavy nuclei as in Appendix A) and electrons. With two possible spectra for each component, we obtain four possible profiles of ζ^{H_2} . These are shown in Fig. 15 as function of $N(\text{H}_2)$, compared with a compilation of empirical determinations of ζ^{H_2} in diffuse and dense clouds. Our data sample includes: (i) diffuse clouds with $N(\text{H}_2)$ from 10^{20} cm^{-2} to 10^{22} cm^{-2} (14 detections and 15 upper limits, from Indriolo et al. 2007, including previous data of McCall et al. 2002) and for the ζ Per line-of-sight (Shaw et al. 2008); (ii) molecular cloud cores with $N(\text{H}_2)$ from 10^{21} cm^{-2} to 10^{22} cm^{-2} (data for low-mass cores from Caselli et al. 1998, Williams et al. 1998, and for the prestellar core B68 from Maret & Bergin 2007); (iii) massive protostellar envelopes with $N(\text{H}_2)$ from 10^{22} cm^{-2} to 10^{23} cm^{-2} (see Table 6 and references therein).

The observational value of ζ^{H_2} in diffuse clouds is obtained from the steady-state abundance of H_3^+ , produced by the CR ionization of H_2 followed by a fast charge exchange reaction with H_2 and destroyed mainly by electron recombination. The situ-

Table 6. CR ionization rate toward massive protostellar envelopes

	$N(\text{H}_2)$ (cm^{-2})	ζ^{H_2} (s^{-1})
NGC 2264 IRS	8.3×10^{22} (a)	$(4 \pm 2) \times 10^{-16}$ (a)
GL 2136	1.2×10^{23} (b)	7.6×10^{-17} (c)
W3 IRS5	1.3×10^{23} (a)	$(4 \pm 2) \times 10^{-17}$ (a)
GL 2591	9.6×10^{22} (d)	1.3×10^{-16} (c)
GL 490	2.0×10^{23} (b)	1.5×10^{-17} (c)
W 33A	6.2×10^{23} (b)	3.0×10^{-17} (c)
W3 IRS5	2.3×10^{23} (b)	6.4×10^{-17} (c)
S 140	1.4×10^{23} (b)	8.5×10^{-17} (c)
DR21(OH)	1.1×10^{23} (e)	3.1×10^{-18} (e)

(a) from de Boisanger, Helmich, & van Dishoeck (1996)

(b) CO column density and CO/ H_2 ratio from van der Tak et al. (2000)

(c) CR rate from van der Tak & van Dishoeck (2000)

(d) from Doty et al. (2002)

(e) from Hezareh et al. (2008)

ation for dense molecular clouds and protostellar envelopes is more complicated. In the dense molecular gas, H_3^+ is removed by reactions with other molecules and atoms of the gas, e.g., by reaction with CO to form HCO^+ and with O to form OH^+ . Thus ζ^{H_2} can be determined from the measured abundance of a variety of molecular ions such as HCO^+ , DCO^+ and N_2H^+ (see e.g. Caselli et al. 1998; van der Tak & van Dishoeck 2000; Doty et al. 2002). The resulting rates are nonetheless very uncertain, as they depend on the depletion of elemental C and O from their cosmic abundances, especially for clouds with a low degree of ionization, and are generally sensitive to the adopted chemical model. Here we adopt the values of ζ^{H_2} derived by Caselli et al. (1998) with the data of Butner, Lada, & Loren (1995) and the chemical model of Leung, Herbst, & Huebner (1984). We view the range of values of ζ^{H_2} obtained for different depletion factors as an indication of the associated uncertainties in the model determinations. In contrast with the study of Caselli et al. (1998), Williams et al. (1998) analyze molecular line data for a sample of low-mass cores using the chemical models of Bergin, Langer & Goldsmith (1995) and Bergin & Langer (1997). They conclude that a single value (or a narrow range of values) of ζ^{H_2} can reproduce reasonably well the observations for the majority of cores in their sample.

The comparison between model results and observational data shown in Fig. 15 should be taken as indicative and interpreted in a statistical sense, as also suggested by the large spread of values of ζ^{H_2} at each value of $N(\text{H}_2)$. First, the *observational* $N(\text{H}_2)$ is the entire column density through the cloud, whereas the *model* $N(\text{H}_2)$ is the column traversed by CRs incident over the cloud’s surface. The exact relation between the quantities depend on factors like the cloud geometry and orientation with respect to the line-of-sight, and the variation of CR ionization rate with depth within the cloud. In addition, for the cloud cores of Caselli et al. (1998) we adopted the H_2 column density estimated by Butner et al. (1995) from measurements of C^{18}O multiplied by a factor of 2, to account for depletion of CO onto grains (Caselli et al. 1998). In fact, at the time of the study by Caselli et al. 1998, the almost complete disappearance of CO from the gas phase *in cloud cores* was still unknown. Second, many of the sight-lines where ζ^{H_2} has been determined in diffuse clouds may have multiple cloud components, which would reduce the column density of a single cloud. It is probably safe to conclude that the *observational* column density is an *upper limit* to the

column density traversed by CRs incident on each cloud, and therefore the data shown in Fig. 15 should probably be shifted to the left by a factor of 2 or so. We will address the problems relative to cloud geometry and the effects of magnetic fields in a subsequent work. At any rate, from the comparison with observational data, shown in Fig. 15, we can draw the following conclusions:

(i) Although the gas column density of the object is by no means the only parameter controlling the CR ionization rate, the data suggest a decreasing trend of ζ^{H_2} with increasing $N(\text{H}_2)$, compatible with our models M02+C00, W98+E00, W98+C00. However, the measured values of ζ^{H_2} are very uncertain, especially in dense environments. Part of the large spread in the sample of cloud cores may be due to a poor understanding of the chemistry.

(ii) The highest values of ζ^{H_2} , measured in diffuse clouds sight lines, could be explained if CR electrons are characterized by a rising spectrum with decreasing energy. The E00 spectrum represents an extreme example of this kind, and it results in values of ζ^{H_2} somewhat in excess of the diffuse clouds observations. The same spectrum accounts simultaneously for the CR ionization rates measured in most protostellar envelopes of much higher column density. Conversely, a spectrum of protons and heavy nuclei rising with decreasing energy, like the M02 spectrum, can provide alone a reasonable lower limit for the CR ionization rate measured in diffuse clouds.

(iii) Without a significant low-energy (below ~ 100 MeV) component of electrons and/or protons and heavy nuclei, it is impossible to reproduce the large majority of observations. The combination of the C00 spectrum for electrons with the W98 spectrum for protons and heavy nuclei clearly fails over the entire range of column densities. Finally, a few molecular cloud cores and one dense envelope characterized by $\zeta^{\text{H}_2} \leq 10^{-17} \text{ s}^{-1}$ can only be explained by invoking the CR suppression mechanisms mentioned in Sect. 1 not considered in this work.

In a recent paper, published after our work was completed, Indriolo, Fields & McCall (2009) analyze the implications of the CR ionization rate measured with H_3^+ in diffuse and dense clouds with an approach similar to that adopted in this paper. As in the present work, Indriolo et al. (2009) reach the conclusion that a low-energy CR component, likely produced by weak, localized shocks, can account for the relatively high CR ionization rate measured in diffuse clouds. However, their “best-fitting” CR-proton spectrum increases below $E_p \approx 100$ MeV as $E_p^{-2.15}$, much more steeply than our steepest spectrum (M02, increasing as E_p^{-1}). Indriolo et al. avoid a too large CR ionization (and heating) rate by cutting off the proton spectrum below $E_p = 2$ MeV and $E_p = 10$ MeV for diffuse and dense clouds, respectively. These energies correspond roughly to proton ranges in H_2 of 10^{21} cm^{-2} and 10^{22} cm^{-2} , respectively. However, our work shows instead that when CR propagation is properly taken into account, low-energy particles are continuously produced by more energetic particles when they slow-down by interacting with the ambient medium (see Sect. 7), making significantly to the ionization rate. In addition, we found that the contribution of CR-electrons to the ionization of H_2 , neglected by Indriolo et al. (2009), can be significant or even dominant over the contribution of CR-protons and heavy nuclei, without violating the available observational constraints.

9. Conclusions

The comparison between our models and the observational data available for diffuse clouds, dense cores and massive protostellar

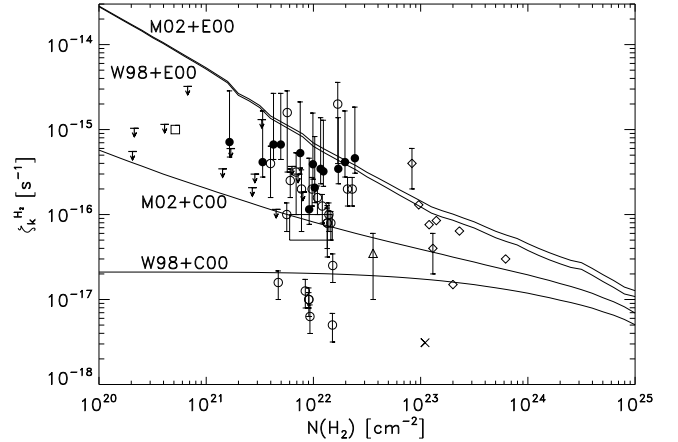


Fig. 15. Total CR ionization rate ζ^{H_2} a function of $N(\text{H}_2)$ according to our models (solid curves). Observational data: filled circles and upper limits, diffuse clouds (Indriolo et al. 2007); square, diffuse cloud towards ζ Per (Shaw et al. 2008); empty circles, dense cores (Caselli et al. 1998); triangle, prestellar core B68 (Maret & Bergin 2007); filled squares, protostellar envelopes (see Table 6 for references); cross massive star-forming region DR21(OH) (Hezareh et al. 2008). The box indicates the range of column densities and CR ionization rates compatible with the data analyzed by Williams et al. (1998).

envelopes indicates that good agreement between theory and observations can be obtained for the CR ionization rate of the ISM by including CR electrons with an energy spectrum increasing towards low energies, as also suggested by Webber (1998). In order to draw more stringent conclusions, it is necessary to use observational constraints derived from the ionization rates of diffuse clouds, as seen in Fig. 15 where the models differ mainly at low column densities. Our study points out the current limits towards a more accurate understanding of the ionization due to cosmic rays. There are essentially two limits: (1) the uncertainty in the CR spectrum at energies below ~ 1 GeV, and (2) the uncertainties in the empirically determined values of ζ^{H_2} in diffuse and dense molecular clouds. The estimates of the ionization rate depend sensitively on the complex set of chemical reactions governing the chemistry of the ISM, particularly on the so-called depletion processes that transfer molecules and ions from the gas phase to the solid phase. Despite these observational uncertainties, several important conclusions clearly emerge from our study:

(i) values of ζ^{H_2} measured in diffuse clouds are greater on average by an order of magnitude than those ones measured in dense molecular clouds. If confirmed, these data imply the presence of a CR proton and/or CR electron spectrum which increases at low energies. Thus, a combination of the spectra W98 and C00 for protons and electrons, respectively, is excluded by this set of observations;

(ii) values of ζ^{H_2} measured in dense molecular clouds span a range of about two orders of magnitude and are subject to considerable uncertainty. It is difficult to establish how much of the observed spread is due to variations in the CR ionization rate. It is likely that in dense clouds the effects of magnetic fields on the propagation of CR particles cannot be neglected. In addition, it might be necessary to take into account the density distribution inside each cloud;

(iii) the values of ζ^{H_2} measured in massive protostellar envelopes are somewhat higher than the predictions of our models at the corresponding column densities. This seems to suggest the presence of further ionization sources in these objects, as, for example, X-ray emission from the young stellar objects;

(iv) The exponential attenuation of the CR ionization rate assumed in many studies is only established for column densities larger than $\sim 10^{25} \text{ cm}^{-2}$. For the lower column densities considered in this work, the ionization rate decreases as $\zeta^{\text{H}_2} \propto N(\text{H}_2)^{-a}$ with $a \approx 0.4\text{--}0.8$ for the spectra that best reproduce the observational data.

It is reasonable to suppose that some of the observational uncertainties discussed here will be removed or reduced in the near future. With respect to the calculation of the ionization rate in dense clouds, the understanding of the complex chemical reactions and of the depletion processes appear to be improving rapidly. Regarding the extrapolation of the measured CR spectra to low energies, the particle fluxes measured by Voyager and Pioneer spacecrafts outside of the solar magnetopause should provide important constraints on the energy distribution of CR protons and CR electrons, and, in any case, improve our understanding of solar modulation.

Acknowledgements. MP and DG acknowledge support from the Marie-Curie Research Training Network ‘‘Constellation’’ (MRTN-CT-2006-035890). AEG acknowledges support from NSF grant AST-0507423 and NASA grant NNG06GF88G. We thank an anonymous referee for insightful comments that helped to improve our paper.

Appendix A: Approximated corrections for heavy-nuclei

In the Bethe-Born approximation, the cross section for the collisional ionization of an atom or molecule depends only on the charge Z_k and the velocity v_k of the incident particle. If A_k is the number of nucleons in the incident particle, the ionization cross section is $\sigma_k(E_k) \approx Z_k^2 \sigma(\epsilon)$, where $\epsilon = E_k/A_k$ is the kinetic energy per nucleon and $\sigma(\epsilon)$ is the same for all particle’s species. If, in addition, the spectra of CR protons and heavy nuclei can be approximately described by a single function $j(\epsilon)$ such that $j_k(E_k) dE_k \approx f_k j(\epsilon) d\epsilon$, with f_k representing the fractional abundance by number of species k , it is possible to reduce the calculation of the ionization rate by heavy-nuclei impact to that of protons, as

$$\sum_{k \geq 1} \int_{I(\text{H}_2)}^{E_{\text{max}}} j_k(E_k) [1 + \phi_k(E_k)] \sigma_k^{\text{ion}}(E_k) dE_k \approx (1 + \eta) \int_{I(\text{H}_2)}^{E_{\text{max}}} j_p(E_p) [1 + \phi_p(E_p)] \sigma_p^{\text{ion}}(E_p) dE_p, \quad (\text{A.1})$$

where η is the correction factor for heavy nuclei ionization,

$$\eta \equiv \sum_{k \geq 2} \frac{f_k}{f_p} Z_k^2. \quad (\text{A.2})$$

Similarly, the correction factor to account for the energy density of heavy nuclei (eq. 17) is given by

$$\xi \equiv \sum_{k \geq 2} \frac{f_k}{f_p} A_k. \quad (\text{A.3})$$

Assuming for the CR abundance of heavy nuclei the standard solar abundance (Anders & Grevesse 1989), we obtain $\eta = 0.51$, and $\xi = 0.41$, in agreement with the values $\eta = 0.50$ and $\xi = 0.42$ of Indriolo et al. (2009).

References

Afrosimov, V. V., Il’in, R. N., Fedorenko, N. V. 1958, Zh. Eksp. Teor. Fiz., 34, 1398 [Sov. Phys.-JETP, 7, 968]
 Anders, E., Grevesse, N. 1989, Geochim. Cosmochim. Acta, 53, 197
 Berezhinskii, V. S., Bulanov, S. V., Dogiel, V. A., Ginzburg, V. L., Ptuskin, V. S. 1990 Astrophysics of Cosmic Rays (North-Holland)
 Bergin, E. A., Langer, W. D., Goldsmith, P. F. 1995, ApJ, 441, 222

Bergin, E. A., Langer, W. D. 1997, ApJ, 486, 316
 Bethe, H. 1933, Handbuch der Physik, Vol. 24 (Berlin: Springer), Pt. 1, p. 491
 Black, J. H., Dalgarno, A. 1977, ApJS, 34, 405
 Black, J. H., Hartquist, T. W., Dalgarno, A. 1978, ApJ, 224, 448
 Butner, H. M., Lada, E. A., Loren, R. B. 1995, ApJ, 448, 207
 Casadei, D., Bindi, V. 2004, ApJ, 612, 262
 Caselli, P., Walmsley, C. M., Terzieva, R., Herbst, E. 1998, ApJ, 499, 234
 Cecchi-Pestellini, C., Aiello, S. 1992, MNRAS, 258, 125
 Cesarski, C. J., Völk, H. J. 1978, A&A, 70, 367
 Chandran, B. D. G. 2000, ApJ, 529, 513
 Colgan, J., Pindzola, M. S., Childers, G., Khakoo, M. A. 2006, Phys. Rev. A., 73, 042710
 Cravens, T. E., Victor, G. A., Dalgarno, A. 1975, Plan. Space Sci., 23, 1059
 Cravens, T. E., Dalgarno, A. 1978, ApJ, 219, 750
 Curran, R., Donahue, T. M., Kasner, W. H. 1959, Physical Review, 114, 490
 Dalgarno, A. 2006, Publ. Nat. Acad. Sci., 103, 12269
 Dalgarno, A., Yan, M., Liu, W. 1999, ApJS, 125, 237
 de Boisanger, C., Helmich, F. P., van Dishoeck, E. F. 1996, ApJ, 463, 181
 deHeer, F. J., Schutzen, J., Moustafa, H. 1966, Physica, 32, 1766
 Doty, S. D., van Dishoeck, E. F., van der Tak, F. F. S., Bonnman, A. M. S. 2002, A&A, 389, 446
 DuBois, R. D., Toburen, L. H., Rudd, M. E. 1984, Phys. Rev. A, 29, 70
 Edwards, A. K., Wood, R. M., Beard, A. S., Ezell, R. L. 1988, Phys. Rev. A, 37, 3697
 Federman, S. R., Weber, J., Lambert, D. L. 1996, ApJ, 463, 181
 Hartquist, T. W., Black, J. H., Dalgarno, A. 1978, MNRAS, 185, 643
 Hartquist, T. W., Doyle, H. T., Dalgarno, A. 1978, A&A, 68, 65
 Gilbody, H. B., Hasted, J. B. 1957, Proc. Roy. Soc. (London) A240, 382
 Hayakawa, S., Nishimura, S., Takayanagi, T. 1961, PASJ, 13, 184
 Geballe, T. R., McCall, B. J., Hinkle, K. H., Oka, T. 1999, ApJ, 510, 251
 Glassgold, A. E., Langer, W. D. 1973a, ApJ, 179, L147
 Glassgold, A. E., Langer, W. D. 1973b, ApJ, 186, 859
 Glassgold, A. E., Langer, W. D. 1974, ApJ, 193, 73
 Heiles, C., Troland, T. H. 2005, ApJ, 624, 773
 Hezareh, T., Houde, M., McCoey, C., Vastel, C., Peng, R. 2008, ApJ, 684, 1221
 Hooper, J. W., McDaniel, E. W., Martin, D. W., Harmer, D. S. 1961, Phys. Rev., 121, 1123
 Indriolo, N., Geballe, T. R., Oka, T., McCall, B. J. 2007, ApJ, 671, 1736
 Indriolo, N., Fields, B. D., & McCall, B. J. 2009, ApJ, 694, 257
 Kossmann, H., Schwarzkopf, O., Schmidt, V. 1990, J. Phys. B, 23, 301
 Kim, Y.-K., Rudd, M. E. 1994, Phys. Rev. A, 50, 3954
 Krishnakumar, E., Srivastava, S. K. 1994, J. Phys. B, 27, L251
 Krollik, J. H., & Kallman, T. R. 1983, ApJ, 267, 610
 Leung, C. M., Herbst, E., Huebner, W. F. 1984, ApJS, 56, 231
 Lindsay, B. G., Mangan, M. A. 2003, in Landolt-Börnstein, 1/17C: Photon and Electron Interactions with Molecules: Ionization and Dissociation, ed. Y. Itikawa (Berlin: Springer), 5-1
 Liu, X., Shemansky, D. E. 2004, ApJ, 614, 1132
 Maret, S., Bergin, E. A. 2007, ApJ, 664, 956
 McCall, B. J., Geballe, T. R., Hinke, K. H., Oka, T. 1998, Science, 279, 1910
 McCall, B. J., Huneycutt, A. J., Saykally, R. J., Geballe, T. R., Djuric, N., Dunn, G. H., Semaniak, J., Novotny, O., Al-Khalili, A., Ehlerding, A., Hellberg, F., Kalthori, S., Neau, A., Thomas, R., Österdahl, F., Larsson, M. 2003, Nature, 422, 500
 McClure, G. W. 1966, Phys. Rev., 148, 47
 McKee, C. F. 1989, ApJ, 345, 782
 Mewaldt, R. A., Wiedenbeck, M. E., Scott, L. M., Binns, W. R., Cummings, A. C., Davis, A. J., Israel, M. H., Leske, R. A., Stone, E. C., von Rosenvinge, T. T. 2004, Physics of the Outer Heliosphere, AIP Conference Proceedings, vol. 719, p. 127
 Montague, R. G., Harrison, M. F. A., Smith, A. C. H. 1984, J. Phys. B, 17, 3295
 Moskalenko, I. V., Strong, A. W., Ormes, J. F., Potgieter, M. S. 2002, ApJ, 565, 280
 Mott, N. F. 1930, Proc. R. Soc. London, 126, 259
 Nakano, T., Tadamaru, E. 1972, ApJ, 173, 87
 Nath, B. B., Biermann, L. 1994, MNRAS, 267, 447
 Padoan, P., Scalzo, 2005, ApJ, 624, L97
 Phelps, A. V. 1990, J. Phys. Chem. Ref. Data, 19, 3
 Pindzola, M. S., Robicheaux, F. J. 2000, Phys. Rev. A., 61, 052507
 Pivovarov, L. I., Levchenko, Y. Z. 1967, Zh. Eksp. Teor. Fiz., 52, 42 [Sov. Phys.-JETP, 25, 27]
 Potgieter, M. S. 1995, Adv. Space Res., 16 (9), 191
 Puckett, L. J., Martin, D. W. 1970, Phys. Rev. A, 1, 1432
 Ramaty, R., & Lingenfelter, R. E. 1975, Solar Gamma-, X-, and EUV Radiation, 68, 363
 Ramaty, R., Kozlovsky, B., & Lingenfelter, R. E. 1996, ApJ, 456, 525
 Rapp, D., Englander-Golden, P. 1965, J. Chem. Phys., 43, 1464
 Rapp, D., Englander-Golden, P., Briglia, D. D. 1965, J. Chem. Phys., 42, 4082

- Rudd, M. E., DuBois, R. D., Toburen, L. H., Ratcliffe, C. A., Goffe, C. W. 1983, *Phys. Rev. A*, 28, 3244
- Rudd, M. E., Kim, Y.-K., Madison, D. H., Gallagher, J. W. 1985, *Rev. Mod. Phys.*, 57, 965
- Rudd, M. E. 1991, *Phys. Rev. A*, 44, 1644
- Schlickeiser, R. 2002, in *Cosmic Ray Astrophysics*, (Springer: Berlin)
- Shah, M. B., Gilbody, H. B. 1985, *J. Phys. B.*, 18, 899
- Shah, M. B., Elliott, D. S., McCallion, P., Gilbody, H. P. 1988, *J. Phys. B*, 21, 2751
- Shaw, G., Ferland, G. J., Srianand, R., Abel, N. P., van Hoof, P. A. M., Stancil, P. C. 2008, *ApJ*, 675, 405
- Silk, J., & Norman, C. 1983, *ApJ*, 272, L49
- Skilling, J., Strong, A. W. 1976, *A&A*, 53, 253
- Spitzer, L., Tomasko, M. G. 1968, *ApJ*, 152, 971
- Straub, H. C., Renault, P., Lindsay, B. G., Smith, K. A., Stebbings, R. F. 1996, *Phys. Rev. A*, 54, 2146
- Strong, A. W., Moskalenko, I. V., Reimer, O. 2000, *ApJ*, 537, 763
- Takayanagi, M. 1973, *PASJ*, 25, 327
- Takayanagi, K., Suzuki, H. 1978, *Cross sections for atomic processes*, vol. I (Nagoya, Institute of Plasma Physics)
- Toburen, L. H., Wilson, W. E. 1972, *Phys. Rev. A*, 5, 247
- Umebayashi, T., Nakano, T. 1981, *PASJ*, 33, 617
- Umebayashi, T., Nakano, T. 2009, *ApJ*, 690, 69
- van Dishoeck, E. F., Black, J. H. 1986, *ApJS*, 62, 109
- van der Tak, F. F. S., van Dishoeck, E. F. 2000, *A&A*, 358, L79
- van der Tak, F. F. S., van Dishoeck, E. F., Evans, N. J., II, Blake, G. A. 2000, *ApJ*, 537, 283
- Van Zyl, B., Stephen, T. M. 1994, *Phys. Rev. A*, 50, 3164
- Wakelam, V., Herbst, E., Selsis, F., Massacrier, G. 2006, *A&A*, 459, 813
- Webber, W. R. 1987, *A&A*, 179, 277
- Webber, W. R. 1998, *ApJ*, 506, 329
- Welsh, L. M., Berkner, K. H., Kaplan, S. N., Pyle, R. V. 1967, *Phys. Rev.*, 158, 85
- Williams, J. P., Bergin, E. A., Caselli, P., Myers, P. C., Plume, R. 1998, *ApJ*, 503, 689